Temporal Consolidation Strategy for Ground-Based Image Displacement Time Series: Application to Glacier Monitoring

Guilhem Marsy, Flavien Vernier, Emmanuel Trouvé, *Senior Member, IEEE*, Xavier Bodin, William Castaings, Andrea Walpersdorf, Emmanuel Malet, and Blaise Girard

***Abstract*—In this article, we present a method for combining image-based displacements to build time series. This method takes advantage of the redundancy of these displacements, which comes from multiple possible combinations between images. The proposed method combines common master series with a different master date to construct a single time series of relative displacements. We were able to test this method on displacements computed using images from a stereo time-lapse device recording images of the Argentière glacier during the summer and fall of 2019. Our method was compared to two other displacement aggregation strategies: a simple common master approach and the classical inversion method. In order to perform this comparison, displacement data from four permanent GPS are used. The results show that our method provides a more accurate time series of relative displacements than those obtained with the other methods. The higher accuracy of the proposed method makes the detection of seasonal variations in glacier velocity possible.**

***Index Terms*—Displacement measurement, glacier monitoring, photogrammetry, time series analysis.**

I. Introduction

In the fields of earth observation and geosciences, the use of images to calculate surface displacements is becoming more and more frequent. There are mainly two types of image acquisition plan: punctual campaigns, as airborne acquisitions or with the help of unmanned aerial vehicle [1], or systematic acquisitions at a given frequency, by using autonomous fixed cameras or satellite images, for instance. The latter is chosen when the variation of the studied surfaces' displacements is the variable of interest. As an example, satellite images can be used to monitor glaciers over a whole region of the world [2], or permafrost deformation in a specific area [3]. More closely, fixed digital cameras can also be used to monitor slope movements such as glaciers, rock glacier, and landslides [4]–[6]. An advantage of systematic image acquisition approaches is to provide redundant displacement information: from a set of n images, up to $n(n-1)$ combinations can be formed to calculate forward and backward displacements. The most straightforward approach to combine these images is the so-called common master (CM) approach, which provides time series of relative displacements: displacements are calculated between a reference image and all the images in the series [4]. The second approach, called leap frog, consists of calculating the displacements between successive images, so if the images are separated by one day, we obtain a chronicle of daily velocity.

However, with these approaches, only $n-1$ combinations out of $n(n-1)$ possible combinations are calculated, which does not allow the use of redundant information to reduce noise or gaps in observations. Indeed, the measurement of displacements by images suffers from different sources of noise, independently of the sensor used. For example, we can cite registration errors, changes in the appearance of the surface to be monitored, noise in the images, weather conditions, etc. To filter noisy displacements, a median filter has been used to calculate yearly glacier velocity on displacement calculated on images separated by one year [2]. A similar approach has been used on landslide images taken the same day [6], [7]. We can also note the use of a temporal median filter applied on depth map differences for the detection of change from stereo time-lapse images [8]. With this kind of methods, only a few image combinations are used, thus, the information redundancy is limited. To overcome this issue and use many image combinations, methods based on the inversion of all the measured displacements have been developed to construct robust time series from Interferometric Synthetic Aperture Radar images [9], optical satellite images [10], [11], and from ground-based stereo time-lapse images [5]. Other methods attempt to model the displacement by making assumptions of linearity or oscillation [12], or by using physical models [13]. However, these methods are not easily transposed from one study site to another.

In a previous work, we have presented a method for calculating time series of displacements, in the case of small temporal

Manuscript received June 11, 2020; revised March 4, 2021 and May 12, 2021; accepted July 10, 2021. Date of publication September 24, 2021; date of current version October 15, 2021. *(Corresponding author: Guilhem Marsy.)*

Guilhem Marsy is with the LISTIC, Univ Savoie Mont Blanc, 74000 Annecy, France, and with EDYTEM, CNRS/Univ Savoie Mont Blanc, 73000 Chambéry, France, and also with TENEVIA, 38240 Meylan, France (e-mail: guilhem.marsy@tenevia.com).

Flavien Vernier, Emmanuel Trouvé, and Blaise Girard are with the LISTIC, Univ Savoie Mont Blanc, 74000 Annecy, France (e-mail: flavien.vernier@univ-smb.fr; emmanuel.trouve@univ-smb.fr; blaise.girard@univ-smb.fr).

Xavier Bodin and Emmanuel Malet are with EDYTEM, CNRS/Univ Savoie Mont Blanc, 73000 Chambéry, France (e-mail: xavier.bodin@univ-smb.fr; emmanuel.malet@univ-smb.fr).

William Castaings is with TENEVIA, 38240 Meylan, France (e-mail: william.castaings@tenevia.com).

Andrea Walpersdorf is with ISTerre, CNRS/Univ Grenoble Alpes, 38000 Grenoble, France (e-mail: andrea.walpersdorf@univ-grenoble-alpes.fr).

Digital Object Identifier 10.1109/JSTARS.2021.3115231

baseline: when it is possible to compute displacements between all the images in the series. This method, based on the median of multiple CM series referred to as MMCMS, has been validated on the displacement series of the Laurichard rock glacier [14]. In this article, we propose to extend this method in the case of larger temporal baselines: when it is not possible to compute displacements between images that are too far apart in time. In Section II, we start by briefly presenting the methods used to compute displacement from images taken by a stereo time-lapse device. Then, we review the MMCMS method and propose its sliding extension (S-MMCMS) to adapt to longer baselines. To evaluate the methods, we use displacement data of the Argentière glacier, computed from a stereo time-lapse device, and GPS measurements for validation purposes. These data are presented in Section III. In Section IV, we propose to detail the results of a comparison between the S-MMCMS method and the CM and inversion methods. Finally, Section V details how displacement time series data can highlight variations in glacier velocity during the measurement period and how a parameter of the S-MMCMS method influences this detection.

II. Methods

The proposed methods can be decomposed into three sub-problems. The first one is the measurement of displacement. Here, we propose to briefly present a method based on images from a stereo time-lapse device. It should be noted that any methods and displacement sources can be used to perform MMCMS and S-MMCMS consolidation methods. The second one is the time series calculation in the context of small temporal baselines. Specifically, when the changes between the first and the last image are small enough to allow the calculation of the displacement between them. The third problem concerns the calculation of time series over long periods of time when it is not possible to calculate shifts between images due to important changes between images. To answer these issues, we propose the MMCMS method to address the first problem, and then we extend it to the S-MMCMS method to solve the second.

A. Displacement From Stereo Time-Lapse Device

In previous work, we have shown that it is possible to compute metric displacements on the surface of gravitational movements using a stereo time-lapse device [15]. This device comprises two fixed and autonomous cameras, recording images of the studied motion automatically and from two different points of view. Once the device is calibrated, the two views are used to reconstruct in 3-D the geometry of the scene. This 3-D reconstruction is calculated for each stereo pair.

In parallel, a sparse optical flow is calculated between two images taken by the same camera but at two different dates. This result is then projected in 3-D using the 3-D models obtained at each date. Thus, a metric displacement on the surface of the studied movement is obtained. It is important to note that, due to the sparse nature of the optical flow used, displacements are not always measured at the same locations. It is necessary to average the displacement vectors over a small area in order to ensure the presence of vectors for any date of the image series. Hence, the displacement between two dates for an area of the glacier is not symmetrical and different results may be obtained, depending on the direction (forward or backward). Details on the methods to calculate displacements using the stereo time-lapse device can be found in [15].

To evaluate the quality of the measured displacement, we propose to use three different metrics. The first one is the quantity of displacement vector obtained in a zone. A low number of vectors indicates a low textured area or a decorrelation in time. The second indicator is the standard deviation of the displacements norm within the zone. A large standard deviation means more significant uncertainty in the calculation of the zone displacement. Finally, the last indicator is the mean of the optical flow error of each vectors within the zone. This error is given by the minimum eigenvalue of the spatial gradient matrix in the formulation given in [16].

B. Small Temporal Baseline Time Series

The first proposed method takes as input all possible relative displacements between images in the series. The idea is to build several relative displacement time series (RDTS) and then combine them into one time series without outliers. We define a RDTS by considering one reference date (the so-called CM), which is used to compute displacement with all the other dates: if the image time series has N different dates and we take $r_j, j \in [0, N-1]$ as the reference date, the associated RDTS is formed by the displacements between all the dates and the date r_j noted $\vec{d}^{(r_j,i)}$: $\vec{d}^{(r_j,0)}$,..., $\vec{d}^{(r_j,i)}$,..., $\vec{d}^{(r_j,N-1)}$.

Let us note that, in the case of measurements without any noise or errors, the difference between 2 RDTS is constant and equal to the displacement between the two reference dates r_j and r_k

$$\vec{d}^{(r_j,r_k)} = \vec{d}^{(r_j,i)} - \vec{d}^{(r_k,i)} \quad \forall i \in [0, N-1]. \tag{1}$$

Taking advantage of this property, it is possible to estimate this offset with a simple mean difference between each point of the two series

$$\vec{\tilde{d}}^{(r_j,r_k)} = \frac{1}{N} \sum_{i=0}^{N-1} \left(\vec{d}^{(r_j,i)} - \vec{d}^{(r_k,i)} \right). \tag{2}$$

Knowing the offset between two RDTS, we can align them to a single reference series r_j, by applying the offset given by (2). We obtain two different measures at each point of the RDTS (see Fig. 1), one directly from the RDTS which has r_j as reference, and one from the RDTS which has reference r_k corrected by the offset estimated between r_j and r_k, noted $\vec{d}_{r_k}^{(r_j,i)}$

$$\vec{d}_{r_k}^{(r_j,i)} = \vec{d}^{(r_k,i)} - \vec{\tilde{d}}^{(r_j,r_k)} \quad \forall i \in [0, N-1]. \tag{3}$$

We can repeat this for all possible reference pairs N and choose one reference date r_{ref} on which all the series are aligned using (3) to get N measures at each point of the RDTS. The results are a consolidated RDTS (noted C-RDTS), which stores

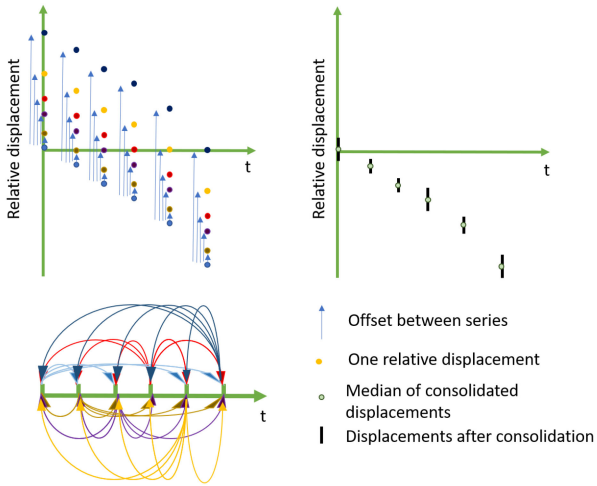

Fig. 1. Time series consolidation principle: relative time series are computed for all reference dates and are consolidated by estimating the offset between them. After consolidation all dates have different measurement coming from the different RDTS (C-RDTS), a unique RDTS is built by taking the median of all measurements in a temporal window.

the following displacements:

$$D_{r_{\text{ref}}}^{(0,1)} = \{\vec{d}_{r_0}^{(0,1)}, \vec{d}_{r_1}^{(0,1)}, \ldots, \vec{d}_{r_N-1}^{(0,1)}\}$$
$$D_{r_{\text{ref}}}^{(0,2)} = \{\vec{d}_{r_0}^{(0,2)}, \vec{d}_{r_1}^{(0,2)}, \ldots, \vec{d}_{r_N-1}^{(0,2)}\}$$
$$\ldots$$
$$D_{r_{\text{ref}}}^{(0,N-1)} = \{\vec{d}_{r_0}^{(0,N-1)}, \vec{d}_{r_1}^{(0,N-1)}, \ldots, \vec{d}_{r_N-1}^{(0,N-1)}\}.$$

To select the reference date r_{ref} on which all the series will be matched, we test all the RDTS as reference and select the one which minimizes the following matching error:

$$\text{error} = \frac{\sum_{i\in N}\sum_{j\in N}\|\vec{d}_{r_{\text{ref}}}^{(0,i)} - \vec{d}_{r_j}^{(0,i)}\|}{N^2}. \quad (4)$$

Then, the marginal median vector (median of each vector component), and the median absolute deviation (MAD) at each date are calculated. A simple threshold on the vector values based on the MAD and the median can be used to detect outliers in the observations. The observations identified as outliers can then be removed from the initial set of observations and the procedure of obtaining C-RDTS can be recomputed without these observations. The offset between the series is more robustly estimated by removing the outliers, leading to less dispersion in the final C-RDTS. A median RDTS with only one measurement per date can be constructed by taking the median of all the displacements within a time frame of a given duration. The longer is the time frame, the smoother RDTS will be. The principle of this algorithm is summarized in Fig. 2 and Algorithm 1.

C. Long Temporal Baseline Time Series

When the temporal baseline is long and involves changes in the images that are too large to calculate displacements between them, it becomes impossible to obtain a reference time series over the entire time period. Let $\Delta t_{\max}$ denotes the maximum

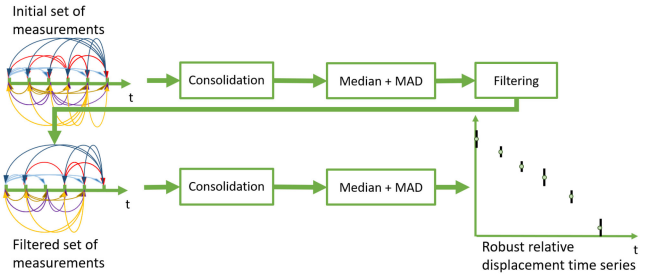

Fig. 2. Complete pipeline to build robust RDTS from redundant displacements. The consolidation step is first applied to the initial set of measurements (see Fig. 1), and then outliers are removed from the initial pool of measurements and the consolidation is recomputed without them.

time between two images for which it is possible to calculate a displacement. We propose to construct the reference series incrementally by applying the MMCMS method on subseries. Starting from a reference date r_{ref} in the series, and for each date in the image series, we apply the MMCMS method to construct a robust sub-RDTS (noted sRDTS) with displacements within $\Delta t_{\max}$. The first sRDTS initialize the beginning of the reference C-RDTS. Then, the sRDTS related to the date $r_{\text{ref}+1}$ and $r_{\text{ref}-1}$ in the series are built with the MMCMS method and are corrected by estimating the offset with the reference series on the common dates with (2). Then, the reference C-RDTS is updated with the median of the corrected sRDTS and previous reference C-RDTS values coming from previous sRDTS, for each displacement $\vec{d}^{\,(r_{\text{ref}},i)}$ when the value is present in each series, or directly with the corrected sRDTS value when the displacement is not present in the reference C-RDTS. This operation is repeated for each date in the image series. The choice of the starting date of the procedure influences the result: if the corresponding sRDTS is affected by an important error, this has repercussions on all the dates. Thus, the date is chosen so that the corresponding sRDTS minimizes the error of (4). This sliding version of the MMCMS algorithm is detailed in Algorithm 2.

It is important to note that if some displacement data are missing, for example, due to snowfall masking the study surface, the maximum time between images for which we calculate a displacement must be greater than the interval without data. Therefore, the parameter $\Delta t_{\max}$ is set according to the maximum duration without data so that the entire time series can be reconstructed with the same reference date. This parameter depends on the site and the dynamics of the studied movement and on the method used to calculate the displacements. If the time without data exceed $\Delta t_{\max}$, each subtime series, before and after missing data, should be processed separately. The metrics described in Section II-A can be used to determine this parameter in the context of a stereo time-lapse device. Section V-B proposes to analyze the influence of this parameter on the result of the S-MMCMS method.

D. Velocity Time Series

MMCMS and S-MMCMS methods make it possible to obtain RDTS. In some cases, the variable of interest is the variations of these displacements over time. It is, therefore, necessary to

Algorithm 1: MMCMS Algorithm.

Data: $DATA$: array of $[\vec{d}^{(i,j)}]$ $\forall i,j \in [0:N[$
Result: A RDTS : array of $[\vec{d}^{(0,i)}]$ $\forall i \in [0:N[$;
Function `buildCM`($DATA$: *array of* $[\vec{d}^{(i,j)}]$ $\forall i,j \in [0:N[$):
  foreach $d_{i-j} \in DATA$ **do**
    $CM[i][j] \leftarrow d_{i-j}$
  end
  return CM;
End Function;
$min_{score} \leftarrow -1$;
$min_{idx} \leftarrow -1$;
CM = buildCM($DATA$);
for $i \leftarrow 0$ **to** $N-1$ **do**
  $error \leftarrow 0$;
  for $j \leftarrow 0$ **to** $N-1$ **do**
    $error \leftarrow error + calcError(CM[i], CM[j])$ (see Equation 4);
  end
  if $min_{score} = -1$ *or* $error < min_{score}$ **then**
    $min_{score} \leftarrow error$;
    $min_{idx} \leftarrow i$;
  end
end
for $i \leftarrow 0$ **to** $N-1$ **do**
  $o \leftarrow$ offset($CM[idx_{min}], CM[i]$) (see Equation 2);
  for $j \leftarrow 0$ **to** $N-1$ **do**
    C-$RDTS[j]$.add($CM[i][j] - o$)
  end
end
for $i \leftarrow 0$ **to** $N-1$ **do**
  $RDTS[i] \leftarrow$median(C-$RDTS[i]$);
end
for $i \leftarrow 0$ **to** $N-1$ **do**
  $RDTS[i] \leftarrow RDTS[i] - RDTS[0]$;
end

Algorithm 2: The Sliding Version of the MMCMS Algorithm.

Data: array of $[\vec{d}^{(i,j)}]$ $\forall i,j \in [0:N[$
Result: A RDTS : array of $[\vec{d}^{(0,i)}]$ $\forall i \in [0:N[$;
Function `getSubSeries`(*array* $DATA$ *of* $[\vec{d}^{(i,j)}]$ $\forall i,j \in [0:N[$, *date*, Δt_{max}):
  foreach $\vec{d}^{(i,j)} \in DATA$ **do**
    if $date - \Delta t_{max} < i < date + \Delta t_{max}$ *and* $date - \Delta t_{max} < j < date + \Delta t_{max}$ **then**
      $sDATA.add(\vec{d}^{(i,j)})$;
    end
  end
  return $sDATA$;
End Function ;
for $i \leftarrow 0$ **to** $N-1$ **do**
  $sRDTS[i] \leftarrow$ MMCMS(getSubSeries($i, \Delta t_{max}$)) ;
  $errors[i] \leftarrow sRDTS[i].error$;
end
$min_{idx} \leftarrow$ indexOfMin($errors$) ;
$RDTS \leftarrow sRDTS[min_{idx}]$;
j $\leftarrow$ max(0, min_{idx}-Δt_{max});
for $k \leftarrow 0$ **to** *len*($sRDTS[min_{idx}]$)-1 **do**
  C-$RDTS[j].add(sRDTS[min_{idx}][k])$;
  j $\leftarrow$ j + 1
end
for $i \leftarrow min_{idx} + 1$ **to** $N-1$ **do**
  j $\leftarrow$ max(0, i-Δt_{max});
  $o \leftarrow$ offset($RDTS, sRDTS[i]$) (see Equation 2);
  for $k \leftarrow 0$ **to** *len*($sRDTS$)-1 **do**
    C-$RDTS[j]$.add($sRDTS[k] - o$);
    $RDTS[j] \leftarrow$median(C-$RDTS[j]$);
    j $\leftarrow$ j + 1
  end
end
for $i \leftarrow min_{idx} - 1$ **to** 0 **do**
  j $\leftarrow$ max(0, i-Δt_{max});
  $o \leftarrow$ offset($RDTS, sRDTS[i]$) (see Equation 2);
  for $k \leftarrow 0$ **to** *len*($sRDTS$)-1 **do**
    C-$RDTS[j]$.add($sRDTS[k] - o$);
    $RDTS[j] \leftarrow$median(C-$RDTS[j]$);
    j $\leftarrow$ j + 1
  end
end

obtain velocity time series from RDTS. Since RDTS displacement measurements can be noisy, it is not always feasible to use a simple discrete derivative that is too sensitive to noise. We propose to use the RDTS to determine an average velocity at each time step. This average velocity is calculated using a linear regression on the displacements calculated over a centered temporal window noted Δt. This temporal window can vary to accentuate the smoothing: the higher Δt is, the more the velocity is averaged.

III. Experimental Data

A. Test Site

The method is tested on displacements calculated from stereo pairs of images taken by a time-lapse device looking at the Argentière glacier (Mont-Blanc massif, France) between July and October 2019. This glacier is one of the most studied glaciers in the Alps, and mass balance measurements have been carried since 1975 [17]. The glacier altitude extends between 3400 m a.s.l. and 1600 m a.s.l. Several transverse profiles are studied along the glacier tongue with ablation stakes and GPS measurement campaigns on a punctual or permanent basis. The time-lapse stereo device is installed in order to measure the displacements around one of the study profiles located at an altitude of 2400 m a.s.l. The equipment's characteristics, the placement of the cameras and the methods are detailed in [15]. The availability of abundant measurements in this area and during this period allows us to obtain comparative measurements in order to evaluate the accuracy of the methods based on the exploitation of the images from the stereo time-lapse device [18].

B. Displacements Data

Displacements vector fields are calculated by a stereo time-lapse pipeline [15]. Five specific interest zones (4 on the glacier,

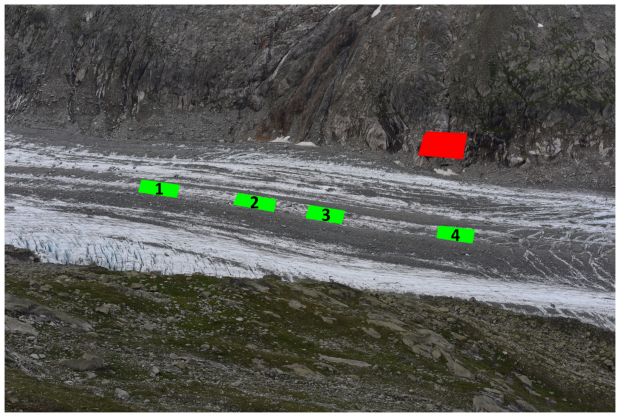

Fig. 3. Localization of the 4 zones on the glacier (in green) and the validation zone over fixed area (in red). The 4 zones are centered around GPS position in the middle of the measurement period.

Fig. 4. Same crop location of images taken in July (top) and October (bottom). The glacier surface has considerably changed and only the biggest boulders are recognizable.

about 10 meters large, and a larger one on a fixed area for uncertainty evaluation) are selected on which a spatial mean displacement vector is calculated for each vector field between two dates. The localization of the zones is presented in Fig. 3. A total of 131 images at different dates are available, but due to ice melt and glacier dynamics, it is not always possible to calculate displacements over a long time period, as illustrated in Fig. 4. To overcome this limitation and apply the S-MMCMS method, a maximum temporal baseline between two images has to be set. There is a tradeoff between a short temporal baseline with highly accurate displacements and a long baseline, which will be more robust to missing images in the dataset.

C. GPS Data

Permanent GPS measurements of the glacier surface are used as a reference [19]. These GPS, which functioned over the entire measurement period, are located on stakes anchored several meters into the ice. Thus, only the horizontal displacement components are comparable since the GPS is not subject to the glacier's surface ablation. Each of the 4 calculation zones corresponds to a GPS position. However, due to the melting of the surface ice and the dynamics of the glacier, the stakes on which the GPS are mounted must be reanchored in the ground periodically to ensure stability. The maintenance of these GPS, therefore, requires a significant amount of field work to ensure continuity of measurement. Thus, there are a few days without GPS data when maintenance could not be carried out.

IV. Results

A. Stereo Displacements

During the ablation period (when the glacier is free of snow), the displacement algorithms mostly track rocks at the glacier surface. When a snowfall occurs, the snow can stay a few days on the glacier surface before it melts, especially during autumn, leading to changes in the texture. During those events, it is not possible to calculate displacements with images before the snowfall, and we have to wait until the snow has completely melted, leading to gaps in the displacements series. If the gap is longer than the maximum time between images to calculate displacements, it will not be possible to build a full RDTS. In our data set, the longest gap is 12 days at the beginning of September, due to bad weather and persistent snow cover.

To determine the maximum time between images ($\Delta t_{\max}$), we calculate all the possible displacements with the first image and record the number of vectors, the standard deviation of the norm and the optical flow mean error over time. A decrease in vector number with a high standard deviation in the norm and an increase in optical flow error are indicators of poor displacements and can be used to choose the maximum time between images. The results on mobile and fixed zones are reported in Fig. 5. A maximal duration of 20 days seems a correct threshold, above, the different indicators on the mobile area differ from those on the fixed zone.

B. Consolidation Methods

To evaluate the method's performance, we compare the results of the RDTS computed from our S-MMCMS method, an inversion method as described in [5] and a simple CM approach with the first image of the series. The three strategies are tested on the same displacement pairs. To quantify the differences, we focus on the displacement over the known fixed zones and the physical coherence of the observed glacier displacement. Indeed, the glacier undergoes a downward gravitational movement, and therefore, the RDTS is a monotonous function. A comparison to GPS measurements is also proposed.

C. RDTS Comparison

In order to deal with the different areas, we chose to estimate the best reference series independently for each of them. On average, each subseries with a maximum deviation of 20 days for each time step represents 1519 pairs of displacements. After the consolidation of these subseries, the average residual error (4) is 6 cm before filtering and 4 cm after, and the average number of displacement pairs per subseries is 750.

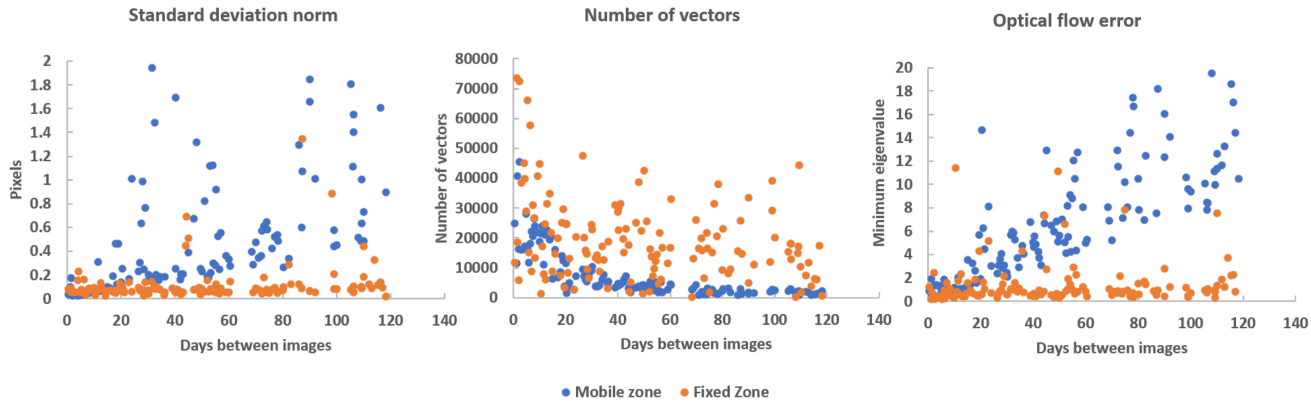

Fig. 5. Different indicators on the displacements computed on the glacier and outside, for different temporal baseline. Above 20 days the standard deviation of the displacement on the considered areas, the number of vectors and the optical flow errors differs significantly from static and fixed areas.

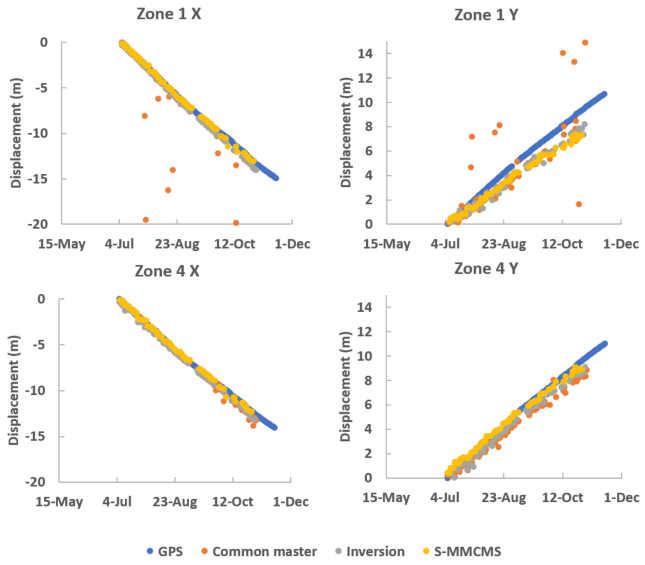

Fig. 6. RDTS of two different zones on the glacier, computed from GPS measurements, CM, inversion and sliding version of the median of multiple common master series (S-MMCMS) strategies. Similar results are observed for all zones situated on the glacier.

We propose several criteria to analyze the performance of the three processing strategies. The first criterion is based on the average displacement norm over the fixed area. It is important to note that the fixed area does not have the same characteristics as the glacier: it is located further away from the cameras, it is less textured and has a different orientation. It is, thus, not possible to extrapolate this average measurement error to the glacier. The second criterion is based on the average velocity of the glacier on the entire measurement period. As shown in Fig. 6, at first order, the glacier is moving at a constant velocity. Therefore, it is possible to compare the average velocity obtained for each of the X and Y components with the three methods and GPS measurements. This comparison indicates whether displacement combination methods can measure first-order glacier dynamics. Another way to evaluate the methods' performance in reducing measurement noise is to analyze the root mean square error (RMSE) between the linear trend and the measurements. To do this, for each area and for each measurement method, we calculate the average velocity using linear regression over the entire measurement period and then calculate the RMSE to this linear trend. The RMSE should be comparable to the one computed from the GPS RDTS. We then propose to evaluate the concordance of the time series with the physical properties of the glacier. The glacier is advancing continuously downstream, so RDTS, which is a cumulative displacement sum, must be a monotonic increasing function (when looking at the flow direction). To check if this physical constraint is respected, we propose to count the number of times the current relative displacement is less than the day before, two days before and up to four days before. The last criterion is based on direct error measurements (RMSE) between GPS RDTS, and RDTS computed from different consolidation methods. The results of the comparisons according to the first three criteria (mean velocities, deviation from linear trend and monotony) are presented in Table I. The RMSE for each consolidation methods and zones regarding the GPS measurements are detailed in Table II.

In the CM case, the displacement over the fixed area is 65 cm, for the inversion method 21 cm and 14.1 cm for S-MMCMS. Our method presents less noise in this area, which is confirmed by the average velocity calculation. Displacements from the CM strategy do not allow the average velocity of the glacier to be measured. The measurements are contaminated by many outliers, which leads to an average absolute difference in velocity compared to GPS over the 4 zones of 13.3 cm/day along X and 9.8 cm/day along Y. On the other hand, inversion and S-MMCMS methods are suitable to measure the average velocity of the glacier over the season with centimetric precision. An absolute difference with average velocity computed from GPS data is measured along X of 0.7 cm/day and 0.4 cm/day for inversion and S-MMCMS, respectively, and according to Y 1.4 cm/day and 0.5 cm/day. When looking at the RMSE of the linear trend, the CM and inversion methods have a significant error, ranging from a few tens of centimeters to several meters. In the case of S-MMCMS method, the error according to X is comparable to GPS (around 10 cm) and larger along Y (around 20 cm). This more significant error according to Y can be explained by the direction of the input displacements

TABLE I
ANALYSIS OF RELATIVE DISPLACEMENTS TIME SERIES ON FOUR DIFFERENT ZONES ON THE GLACIER FROM GPS MEASUREMENTS AND COMPUTED FROM CM, INVERSION, AND SLIDING VERSION OF THE MEDIAN OF MULTIPLE COMMON MASTER SERIES STRATEGIES (S-MMCMS)

	Zone 1	Zone 2	Zone 3	Zone 4
GPS Vmean X (cm/day)	-11.2	-11.6	-10.6	-9.9
GPS Vmean Y (cm/day)	8	8.3	8.3	7.7
CM Vmean X (cm/day)	-20.1	-12.4	-11.5	3.3
CM Vmean Y (cm/day)	6.5	7.5	9.5	-27.5
Inversion Vmean X (cm/day)	-11.9	-11.8	-11.3	-11.1
Inversion Vmean Y (cm/day)	6	6.9	7.2	6.4
S-MMCMS Vmean X (cm/day)	-11.8	-11.5	-10.9	-10.6
S-MMCMS Vmean Y (cm/day)	7.2	7.7	7.9	7.2
GPS RMSE X (cm)	14.8	23.3	13.6	13.6
GPS RMSE Y (cm)	11	13.2	13.6	13.6
CM RMSE X (cm)	877.5	915	19.7	1300
CM RMSE Y (cm)	530.5	528.2	28.5	1300
Inversion RMSE X (cm)	41.1	68.5	84.3	112.5
Inversion RMSE Y (cm)	283.3	254.4	243.9	209.4
S-MMCMS RMSE X (cm)	17.5	17.4	15.7	15.4
S-MMCMS RMSE Y (cm)	27.9	22.7	22.9	18.7
GPS $\|\vec{d}_{0-i}\| < \|\vec{d}_{0-i-1}\|$	0%	0%	0%	0%
GPS $\|\vec{d}_{0-i}\| < \|\vec{d}_{0-i-2}\|$	0%	0%	0%	0%
GPS $\|\vec{d}_{0-i}\| < \|\vec{d}_{0-i-3}\|$	0%	0%	0%	0%
GPS $\|\vec{d}_{0-i}\| < \|\vec{d}_{0-i-4}\|$	0%	0%	0%	0%
CM $\|\vec{d}_{0-i}\| < \|\vec{d}_{0-i-1}\|$	28.2%	18.3%	9.9%	29%
CM $\|\vec{d}_{0-i}\| < \|\vec{d}_{0-i-2}\|$	19.8%	9.9%	7.6%	26.7%
CM $\|\vec{d}_{0-i}\| < \|\vec{d}_{0-i-3}\|$	16%	8.4%	3.8%	25.2%
CM $\|\vec{d}_{0-i}\| < \|\vec{d}_{0-i-4}\|$	16%	8.4%	3.8%	25.2%
Inversion $\|\vec{d}_{0-i}\| < \|\vec{d}_{0-i-1}\|$	13.9%	8.1%	8.1%	2.3%
Inversion $\|\vec{d}_{0-i}\| < \|\vec{d}_{0-i-2}\|$	2.3%	1.2%	2.3%	0%
Inversion $\|\vec{d}_{0-i}\| < \|\vec{d}_{0-i-3}\|$	1.2%	3.5%	2.4%	1.2%
Inversion $\|\vec{d}_{0-i}\| < \|\vec{d}_{0-i-4}\|$	0%	0%	2.7%	0%
S-MMCS $\|\vec{d}_{0-i}\| < \|\vec{d}_{0-i-1}\|$	2.8%	0%	0%	0%
S-MMCS $\|\vec{d}_{0-i}\| < \|\vec{d}_{0-i-2}\|$	0%	0%	0%	0%
S-MMCS $\|\vec{d}_{0-i}\| < \|\vec{d}_{0-i-3}\|$	0%	0%	0%	0%
S-MMCS $\|\vec{d}_{0-i}\| < \|\vec{d}_{0-i-4}\|$	0%	0%	0%	0%

The average velocity (Vmean) calculated by linear regression on the entire period is presented, as well as the RMSE to this linear trend. Monotonicity is assessed by counting the number of times the norm of the current displacement is less than the displacement of the previous days.

TABLE II
RMSE (CENTIMETERS) TO THE GPS MEASUREMENTS FOR EACH RDTS COMPUTED FROM CM, INVERSION AND SLIDING MEDIAN OF MULTIPLE COMMON MASTERS SERIES STRATEGIES (S-MMCMS)

	Zone 1	Zone 2	Zone 3	Zone 4
CM X	1047	954	158	2279
CM Y	753	684	428	2199
Inversion X	117	66	43	50
Inversion Y	87	72	63	65
S-MMCMS X	**22.7**	**22.7**	**17.5**	**25.4**
S-MMCMS Y	**52.5**	**38.5**	**26.7**	**28.9**

Bold entities correspond to the lowest RMSE of all methods

that are more noisy according to this component. Indeed, the displacements come from a time-lapse stereo system whose cameras have viewing direction mainly oriented according to the Y component. The uncertainty is higher according to the viewing axes because of the triangulation in space whose error increases quadratically with depth. Concerning the physical consistency of the measured displacement, GPS measurements and displacement computed from our S-MMCMS method, the RDTS are indeed monotonic increasing functions for each area, with one exception for an area with the S-MMCMS method. In the case of the inversion and CM method, this property is not respected. Finally, the RMSE to the GPS data averaged over all areas is 1110 cm in X direction, 99 cm and 22 cm for the CM, inversion and S-MMCMS approaches, respectively. In Y the corresponding error is 1016 cm, 247 cm, and 37 cm.

V. ANALYSIS

A. Velocity Time Series Comparison

The results presented in Section IV-C allow an evaluation of time series of relative displacements. In the first order, we observe that the glacier velocity is constant over time and that methods (inversion and S-MMCMS) based on the temporal redundancy of the pairs of displacements are necessary to measure this velocity. However, stereo time-lapse devices for monitoring the glacier at daily time steps may be useful to highlight the variations that may occur in second order. Thus, it is interesting to determine whether temporal consolidation methods allow us to observe variations in velocity during the summer and the temporal order of magnitude of these changes: daily, weekly, or monthly variations. The difficulty lies in the fact that these variations, on different time scales, have different amplitudes.

In order to determine at which time scales the consolidation methods can highlight variations in glacier velocities, we propose to compare the velocities obtained with the method described in Section II-D and different levels of temporal smoothing (Δt) between the consolidation methods and the GPS data. This processing is applied to both GPS data and time series obtained by inversion and the S-MMCMS methods for each zone. The time series obtained using the CM strategy is not used because of its noise level, which does not even allow the determination of the average speed over the entire measurement series with precision. It is then possible to compare the velocity time series by calculating the RMSE with the velocity series from the GPS data. In order to obtain an indicator of the amplitude of the velocity variations during the season and for the different levels of smoothing, we use the difference between the minimum and maximum velocity measured by the GPS. Thus, for a temporal smoothing level, if the RMSE between the series resulting from one of the two consolidation methods is less than this maximum difference, it means that the temporal consolidation methods can detect velocity variations on this temporal smoothing scale. Thus, we can plot, for the inversion method and the S-MMCMS method, the evolution of the RMSE and the maximum difference in velocity in the series derived from GPS data as a function of the maximum time between the time step considered and the displacements used to perform the linear regression.

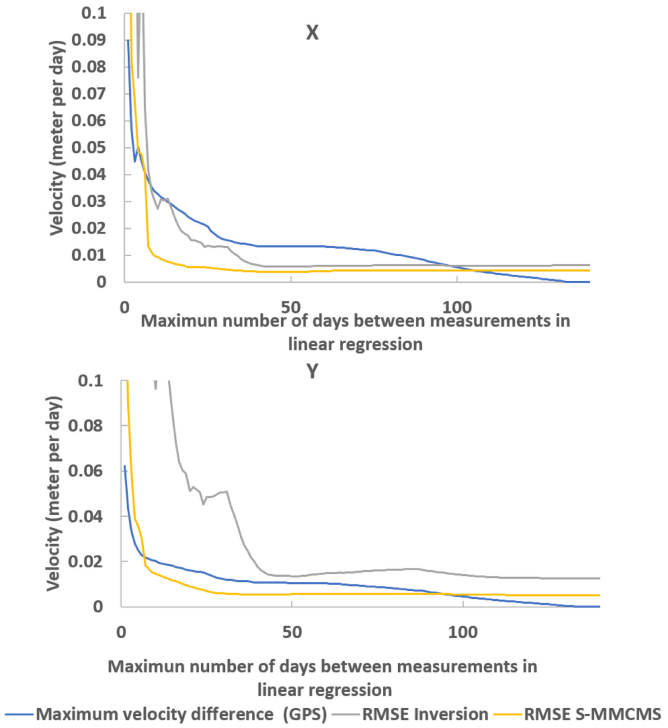

Fig. 7. RMSE of velocity time series computed from inversion and S-MMCMS series to GPS velocity for different temporal velocity smoothing and for both X and Y components.

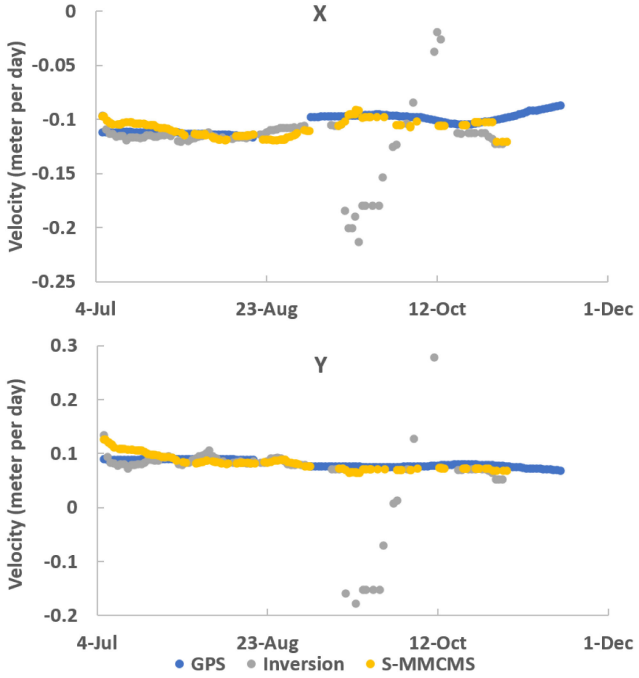

Fig. 8. Velocity time series of the second zone on the glacier, computed from GPS measurements, inversion and sliding version of the median of multiple common master series (S-MMCMS) strategies. Each velocity point has been calculated by linear regression on displacements separated by at most 15 days.

The results are presented in Fig. 7. These results show that the S-MMCMS method gives velocities closer to those measured by the GPS than the inversion method for any temporal smoothing. Moreover, the accuracy seems to be better on the X component, whatever the smoothing is. This is in agreement with the comparison data on time series of relative displacements. Finally, in the case of the S-MMCMS method, the difference between the RMSE and the maximum velocity difference becomes significant for a maximum range of 10 days, i.e., for a speed calculated over a maximum of 20 days (10 days before and 10 days after), for both dimensions. In the inversion method, this difference is significant only beyond 40 days range for the X dimension, whereas in the case of the Y direction the error is greater than the maximum variation. Given the measurement period of 135 days, only the S-MMCMS method seems to be able to detect seasonal trends in velocity. Thus, Fig. 8 presents the time series of speeds over Zone 2 from GPS data, using the inversion and S-MMCMS methods, with a smoothing over a maximum range of 15 days (smoothing over a maximum of one month). The noise present in the inversion method results makes detecting the glacier deceleration that occurs in fall impossible, whereas it is perceived by the S-MMCMS method.

B. Sliding Window Size Influence

At the beginning of this section, we justified the choice of the $\Delta t_{\max}$ parameter at 20 days, by comparing the characteristics of the displacements on the fixed and moving zones according to the duration between the images. With the GPS data as a reference, it is possible to evaluate this parameter's importance

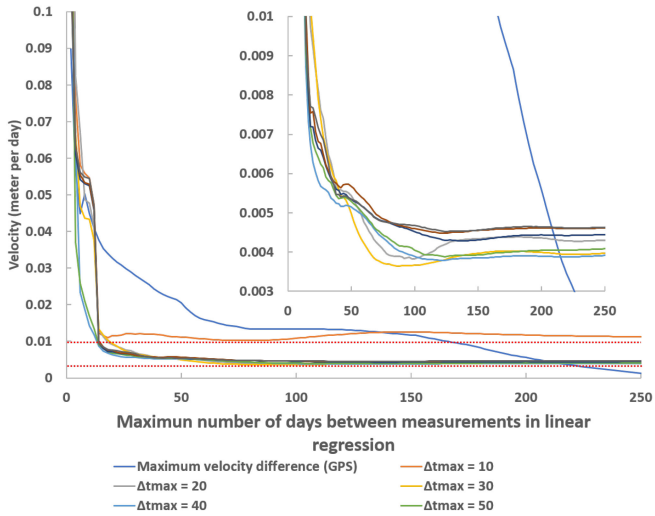

Fig. 9. RMSE of velocity time series computed from S-MMCMS series to GPS velocity for different temporal velocity smoothing and value of $\Delta t_{\max}$ parameters in S-MMCMS method. A zoom on the range 0.003–0.01 is present on the top right corner.

on the deviation from the reference measurement. To do so, we can perform the same analysis as shown in Fig. 7 for different values of this parameter. This analysis is presented in Fig. 9. It is interesting to note that the error on the average glacier velocity value is not very dependent on this parameter: it varies from 4.6 mm/day for a $\Delta t_{\max}$ of 110 days, to 3.9 mm/day for a $\Delta t_{\max}$ of 20 days. In the case of weekly to monthly velocities, similar differences are measured between the different values of $\Delta t_{\max}$. The difference is only significant for a $\Delta t_{\max}$ of 10 days.

This can be explained by the fact that the longest period without measurements lasts 12 days due to the presence of snow on the glacier. A $\Delta t_{\max}$ of 10 days is not enough to overcome such a gap. It can, therefore, be concluded that the S-MMCMS method is sufficiently robust to uncertain displacements and that the maximum time between two images to calculate a displacement has little influence on the resulting time series as long as it is long enough to overcome long missing data periods.

VI. Conclusion

In this article, we proposed a sliding version of the median of multiple common master series (S-MMCMS) method to combine displacements measurements computed from long image time series in order to build a robust time series of relative displacements. The performances of the proposed method are illustrated on a photogrammetric dataset over the Argentière glacier, where a simple common master approach is not sufficient to determine the average glacier velocity with precision. Comparison with the inversion consolidation method, using data from permanent GPS, shows that our method produces a time series of relative displacements with a better signal to noise ratio. While both methods can determine with centimeter accuracy the value of the average glacier velocity over the measurement period, only our method can be used to detect seasonal velocity variations. Indeed, the computation of a velocity time series from the relative displacements time series requires a derivative that is sensitive to noise. We were able to show that our method can detect changes in velocity on a scale of about 20 days. Thus, it is possible to observe the slowing down of the glacier that occurs during the autumn. Future work could focus on using the displacements computed from images over the entire glacier to highlight possible spatial differences in the seasonal dynamics of the glacier. Finally, the joint use of GPS and image data could be used to calculate the evolution of the mass balance during the season.

References

[1] T. Li, B. Zhang, W. Xiao, X. Cheng, Z. Li, and J. Zhao, "UAV-based photogrammetry and LiDAR for the characterization of ice morphology evolution," *IEEE J. Sel. Topics Appl. Earth Observ. Remote Sens.*, vol. 13, pp. 4188–4199, 2020, doi: 10.1109/JSTARS.2020.3010069.

[2] A. Dehecq, N. Gourmelen, and E. Trouvé, "Deriving large-scale glacier velocities from a complete satellite archive: Application to the Pamir-Karakoram-Himalaya," *Remote Sens. Environ.*, vol. 162, pp. 55–66, 2015.

[3] Z. Zhang, M. Wang, X. Liu, C. Wang, and H. Zhang, "Map and quantify the ground deformation around Salt lake in Hoh Xil, Qinghai-Tibet plateau using time-series InSAR from 2006 to 2018," *IEEE J. Sel. Topics Appl. Earth Observ. Remote Sens.*, vol. 14, pp. 858–869, 2021, doi: 10.1109/JSTARS.2020.3031893.

[4] R. Kenner, M. Phillips, P. Limpach, J. Beutel, and M. Hiller, "Monitoring mass movements using georeferenced time-lapse photography: Ritigraben rock glacier, Western Swiss Alps," *Cold Regions Sci. Technol.*, vol. 145, pp. 127–134, Jan. 2018.

[5] H. Hadhri, F. Vernier, Abdourrahmane M. Atto, and E. Trouvé, "Time-lapse optical flow regularization for geophysical complex phenomena monitoring," *ISPRS J. Photogrammetry Remote Sens.*, vol. 150, pp. 135–156, 2019.

[6] M. Desrues, J.-P. Malet, O. Brenguier, J. Point, A. Stumpf, and L. Lorier, "TSM-tracing surface motion: A generic toolbox for analyzing ground-based image time series of slope deformation," *Remote Sens.*, vol. 11, no. 19, pp. 2189–2212, 2019.

[7] A. Stumpf, J.-P. Malet, and C. Delacourt, "Correlation of satellite image time-series for the detection and monitoring of slow-moving landslides," *Remote Sens. Environ.*, vol. 189, pp. 40–55, 2017.

[8] A. Eltner, A. Kaiser, A. Abellan, and M. Schindewolf, "Time lapse structure-from-motion photogrammetry for continuous geomorphic monitoring," *Earth Surface Processes Landforms*, vol. 42, no. 14, pp. 2240–2253, 2017.

[9] M.-P. Doin *et al.*, "Presentation of the small baseline NSBAS processing chain on a case example: The Etna deformation monitoring from 2003 to 2010 using Envisat data," in *Proc. Fringe Symp.*, 2011, pp. 3434–3437.

[10] N. Bontemps, P. Lacroix, and M.-P. Doin, "Inversion of deformation fields time-series from optical images, and application to the long term kinematics of slow-moving landslides in Peru," *Remote Sens. Environ.*, vol. 210, pp. 144–158, 2018.

[11] B. Altena, T. M. S. Fahnestock, and A. Kääb, "Extracting recent short-term glacier velocity evolution over southern Alaska and the Yukon from a large collection of Landsat data," *Cryosphere*, vol. 13, no. 3, pp. 795–814, 2019.

[12] P. Lacroix, G. Araujo, J. Hollingsworth, and E. Taipe, "Self-entrainment motion of a slow-moving landslide inferred from Landsat-8 time series," *J. Geophysical Res., Earth Surf.*, vol. 124, no. 5, pp. 1201–1216, 2019.

[13] O. Maksymiuk, C. Mayer, and U. Stilla, "Velocity estimation of glaciers with physically-based spatial regularization-experiments using satellite SAR intensity images," *Remote Sens. Environ.*, vol. 172, pp. 190–204, 2016.

[14] G. Marsy, F. Vernier, X. Bodin, W. Castaings, and E. Trouvé, "Temporal consolidation strategy for ground based image displacement time series," in *Proc. IEEE Int. Geosci. Remote Sens. Symp.*, Waikoloa, HI, USA, 2020, pp. 132–135.

[15] G. Marsy, F. Vernier, X. Bodin, W. Castaings, and E. Trouvé, "Monitoring mountain cryosphere dynamics by time lapse stereo photogrammetry," *ISPRS Ann. Photogrammetry, Remote Sens. Spatial Inf. Sci.*, vol. V-2-2020, pp. 459–466, 2020.

[16] Jean-Yves Bouguet *et al.*, "Pyramidal implementation of the affine Lucas Kanade feature tracker description of the algorithm," Intel Corporation, vol. 5, no. 1–10, pp. 4–13, 2001.

[17] C. Vincent, A. Soruco, D. Six, and E. L. Meur, "Glacier thickening and decay analysis from 50 years of glaciological observations performed on Glacier d'Argentiére, Mont Blanc area, France," *Ann. glaciol.*, vol. 50, no. 50, pp. 73–79, 2009.

[18] L. Benoit *et al.*, "Multi-method monitoring of Glacier d'Argentiére dynamics," *Ann. Glaciol.*, vol. 56, no. 70, pp. 118–128, 2015.

[19] F. Ponton *et al.*, "Observation of the Argentière Glacier flow variability from 2009 to 2011 by TerraSAR-X and GPS displacement measurements," *IEEE J. Sel. Topics Appl. Earth Observ. Remote Sens.*, vol. 7, no. 8, pp. 3274–3284, Aug. 2014.

Guilhem Marsy received the master's in degree computer science from the University Savoie Mont-Blanc, Polytech Annecy Chambéry, France, in 2016, and the Ph.D. degree in computer vision from the University Savoie Mont-Blanc France, Chambéry, France, in 2020.

During his Ph.D thesis (2017–2020), he was with the Laboratoire, d'Informatique, Systémes, Traitement de l'Information et de la Connaissance, Annecy, France, the Laboratoire EDYTEM, Chambéry, France, and TENEVIA an SME, Meylan, France. His main research interests are glacier and river monitoring based on computer vision.

Flavien Vernier received the master's degree in 2001 and the Ph.D. degree in 2004 from the LIFC Laboratory, University of Franche-Comté, Besançon, France.

Between 2005 and 2006, he joined the ALGORILLE Research Team, LORIA laboratory. Since 2006, he has been an Associate Professor with the LISTIC Laboratory, University of Savoie, Polytech Annecy-Chambéry, France. His research interests concern distributed systems and algorithms. According to these interests, he studies the scientific work flow of image processing for geoscience. In 2005, he introduces the concept of wise object dedicated to self-knowledge acquisition, management and analysis for smart and adaptive systems.

Emmanuel Trouvé (Senior Member, IEEE) received the Ph.D. degree in signal and image processing from Ecole Nationale Supérieure des Télécommunications, Paris, France, in 1996.

He has been working with the University Savoie Mont Blanc, Chambéry, France, Polytech Annecy-Chambéry, Annecy, France, Laboratoire d'Informatique, Saint-Martin-d'Hères, France, Systémes, Traitement de l'Information et de la Connaissance, as an Associate Professor (1998–2008), then as a Professor of Signal and Image Processing. His research interests include synthetic aperture radar (SAR) image processing, photogrammetry and glacier monitoring by remote sensing.

Prof. Trouvé was the General Chair of MultiTemp 2015 (8th International Workshop on the Analysis of Multitemporal Remote Sensing Images).

Andrea Walpersdorf received the Ph.D. degree in geophysics from ENS Paris, Paris, France in 1997, and the Habilitation degree in 2008 from the University Joseph Fourier, Grenoble, France.

She is currently an Observatory Physicist with the Grenoble Observatory for Earth and Universe Sciences, Institute for Earth Sciences (ISTerre), Giéres, France. Since 2017, she is an Executive Director of the French national seismological and geodetic network Resif. Her research interests are high precision GNSS positioning with applications in active tectonics (slow deformation in the Alps, regional deformation and fault slip rates in Iran, silent earthquakes in Mexico, transient deformation in Kamchatka), glacier dynamics from the interannual to the subdaily time scale, and GPS methodology (meteorology and tropospheric corrections of satellite radar images).

Xavier Bodin received the Ph.D. degree in geography from the University Paris-Denis Diderot, Paris, France, in 2007.

Since 2010, he is currently a CNRS Junior Researcher (chargé de recherche) with EDYTEM (Environnements, Dynamiques et Territoires de la Montagne, UMR 5204, CNRS Université Savoie Mont-Blanc), Le Bourget-du-Lac, France. As mountain geomorphologist, his main research interests mostly cover the study of Alpine and Andean permafrost, and more specifically rock glaciers dynamics, in a perspective of improving our understanding of the consequences of environmental changes on high mountain processes.

Emmanuel Malet received the BTS degree in industrial computing from Lycée du Grésivaudan Meylan France in 1994.

He worked for a few years in a design office in automation and robotics. In 2002, he joined the LENA laboratory (University of Lyon 1) to work on instrumentation on ecology and in 2007, the EDYTEM laboratory to work on monitoring permafrost (to study climate change), karst (hydrogeology and pollutions), and lakes (climate change and sedimentology)

William Castaings received the Ph.D. degree in applied mathematics from Grenoble-Alpes University, Grenoble, France in 2007.

He carried out academic research activities in various places (French research institute for digital sciences—INRIA, European Commission Joint research center—JRC, Fluid Mechanics Institute of Toulouse—IMFT), Environment, Dynamics and Mountain Territories Laboratory—EDYTEM). Since 2012, he has been Managing Research and Development with TENEVIA an SME working on measuring, monitoring and forecasting in the water, energy, and environment. His main research interest are river monitoring and hydrological forecasting, computer vision and image processing, sensitivity and uncertainty analysis, data assimilation.

Blaise GIRARD received the BTS degree in design of industrial products in 1994.

Since 2007, he has been a Technician with the LISTIC Laboratory, University of Savoie, Polytech Annecy-Chambéry, France. His work consists to design and install scientific instrumentation in order to monitor alpine glaciers.